Contents lists available at ScienceDirect

Nuclear Materials and Energy

journal homepage: www.elsevier.com/locate/nme

The microstructural in-sight to the mechanical behavior of alumina after high energy proton irradiation

Juan Mauricio Garcia [*], María González , Marcelo Roldan , Fernando Sánchez

Fusion National Laboratory, CIEMAT, Avenida Complutense, 40, 28040 Madrid, Spain

ABSTRACT

The mechanical behaviour of prismatic bars extracted from a high purity alumina tube was studied comparatively in the as-received condition and after being irradiated with high-energy protons. For this study, ten samples were irradiated with 8 MeV H^+ ion beams up to a fluence of 1.63×10^{16} ions/cm^2. Values of compressive strength, elastic modulus, hardness, and fracture toughness were determined from compression and micro-indentation tests. After the mechanical tests, the relationship of the mechanical behaviour shown with the microstructure was considered by scanning electron microscopy (SEM) and transmission electron microscopy (TEM). A clear trend was observed, compressive strength and elastic modulus were considerably reduced, while hardness and fracture toughness increased. This change is attributed to radiation-induced cavities and dislocation loops after high-energy ion-irradiation.

Introduction

Alumina is one of the insulating materials broadly studied for different nuclear fusion applications. Flow Channel Inserts (FCI) for the dual coolant lead–lithium (DCLL) breeding blanket concept [1,2] is another promising application. The excellent high electrical resistivity of a FCI alumina component would considerably reduce the magneto-hydrodynamic effects produced by the movement of the liquid metal along the steel channels under the influence of the strong magnetic field of fusion reactor magnets [3]. Extreme operating conditions are expected for BB components, leading to possible degradation of the material physical properties. Since long-term exposure to high-energy would produce gaseous species due to the transmutation of matrix elements [4,5]. The transmuted hydrogen stimulates nucleation and growth of cavities, which would trigger internal stresses in the ceramic material, thus changing its initial mechanical properties [6]. Therefore, the characterization of the mechanical behaviour in irradiated ceramics is essential since the material would have to fulfill some structural functionality in the most recent DCLL design, based on a single-module segment (SMS) architecture [7,8].

This work aimed to study the mechanical behaviour under compression and micro-indentation tests of high purity alumina material, comparing the as-received condition and high-energy proton material irradiated conditions, accompanying the likely radiation-induced

radiation-induced tests microstructural changes with SEM and TEM observations.

Experimental procedure

Samples for the mechanical tests were extracted from a square section tube of high purity and high density (99.7%, 3.95 g/cm^3) alumina ceramic produced by the slip casting method. Cutting was performed with a diamond disc on a low-speed IsoMet precision cutting machine. Twenty prismatic-bar shape samples were obtained, with dimensional characteristics of 27 mm long, 3 mm wide, and 500 μm thick. Cut samples were polished up to a thickness of 250 μm in a Logitech PM4 precision lapping & polishing machine. Subsequently, thermal annealing at 400 °C for 60 h was applied to reduce the stress likely produced during cutting and polishing that could affect the mechanical behaviour of the ceramic samples.

Ten alumina samples (first group named as Al$_2$O$_3$-AR) were not treated at all. The remaining ten samples (the hereafter called Al$_2$O$_3$-8 MeV) were irradiated with 8 MeV protons up to a total fluence of 1.63×10^{16} ions/cm^2 in the implantation line of the CMAM̈s (Centre for Micro Analysis of Materials) high-energy accelerator [9].

To allow the total transmission of ions through the alumina samples, beam energy and sample thickness were determined by SRIM. The radiation calculated damage (dpa, or displacement per atom) and the ion-
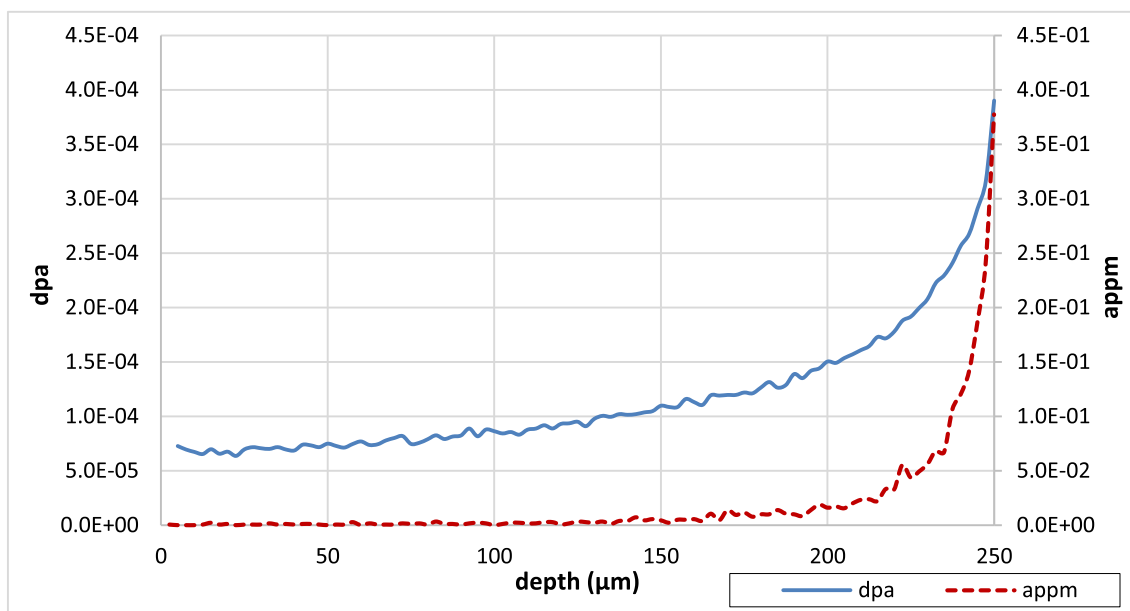
Fig. 1. Radiation damage (in dpa, solid blue line) and implanted hydrogen concentration (in appm, dashed red line) evolution as a function of specimen thickness estimated by SRIM 2013. (For interpretation of the references to colour in this figure legend, the reader is referred to the web version of this article.)
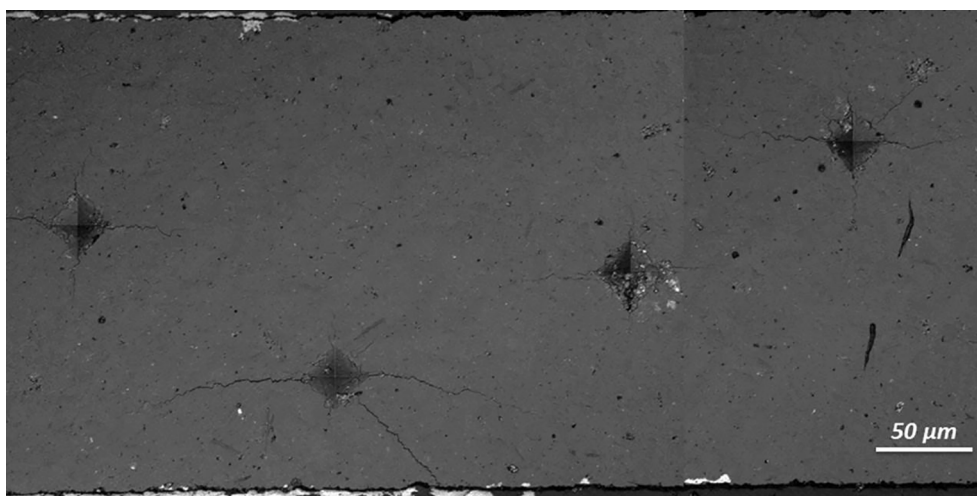
Fig. 2. Alumina probe mounted in an epoxy resin and polished in cross-section, four micro-indentations performed at different thickness positions are shown, to check the mechanical response with the ion penetration distance.

implanted concentration (appm) as a function of specimen thickness is plotted in Fig. 1. Values were obtained based on the method proposed by Stoller [10], applying selected displacement energy values (Ed-Al = 24 eV, Ed-O = 79 eV of Al and O in alumina, respectively [11]) and using full-cascade (FC) damage simulation [12,13]. The maximum values for radiation damage and ion-implanted concentration (3.5×10^{-4} dpa and 3.5×10^{-1} appm, respectively) are then determined to fit sample thickness.

For mechanical characterization, compression tests were performed using a Kammrath & Weiss microtensile/compression module mounted with a load cell of 1 kN and working at a loading rate of 0.2 N/s. Also, micro-indentation tests were performed using a Vickers LV700AT LECO hardness tester, with a force of 9.8 N and a dwell time of 14 s. Prior to be tested, the specimens were embedded in an epoxy resin in such a way that the cross-section is exposed to diamond polishing, ending with a 0.1 μm acidic alumina suspension. Indentations were then performed in the cross-section of polished prismatic samples at different distances

from the ion beam incident surface, as shown in Fig. 2. Afterwards, the imprint size and the crack length were measured with the aid of a Leica DCM8 confocal microscope to determine the material hardness and fracture toughness.

Prior to the microstructural study, mirror-like polished ceramic samples were subjected to a thermal etching method (15 min at 1450 °C) to reveal the grain boundaries. Due to the insulating nature of alumina, a thin film of carbon was sputtered to avoid charging effects during SEM microstructural studies. An Auriga Compact field-emission scanning electron microscope (FESEM) was used to observe the microstructure of polished and etched samples. The samples were checked along the cross-section for possible microstructural changes induced by the high-energy proton irradiation. The images taken were digitally processed with Leyca LAS 4.6 software to determine the grain size of alumina ceramics.

A TEM study was required to continue with the microstructural characterization of the irradiated alumina. A FEI FIB-FESEM cross-beam microscope located at the Laboratorio de Microscopía Avanzada (LMA)
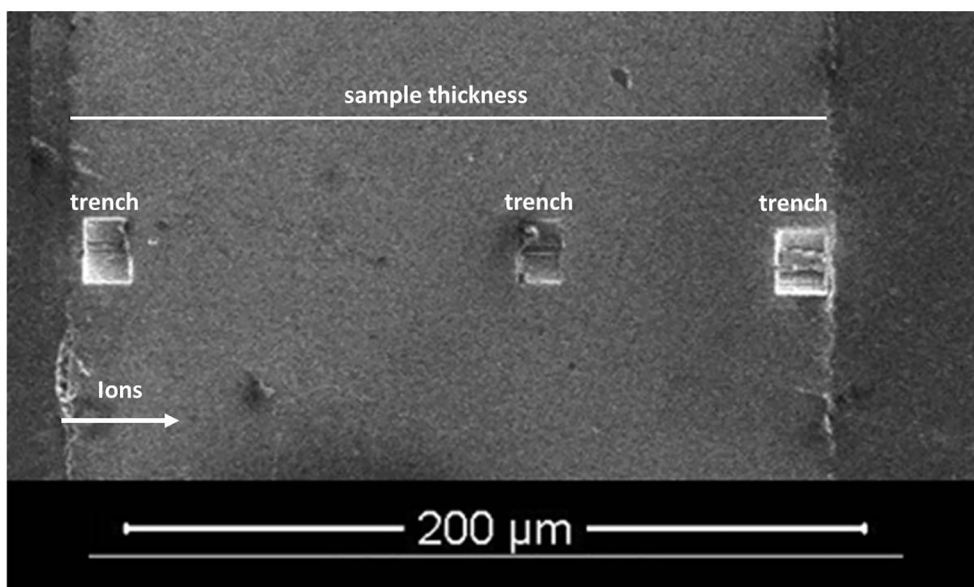
Fig. 3. Position of FIB trenches within the cross-section preparation of the ion-irradiated alumina sample after the TEM lamellae milling.

Table 1
Summary of calculated values of main mechanical parameters obtained from compression tests.

Al_2O_3	σ_C (MPa)	E_C (GPa)	Elastic Energy (kJ/m^3)	Weilbul Modulus
AR	303 ± 86	442 ± 193	486 ± 88	3.9
8 MeV	28 ± 14	35 ± 13	46 ± 16	2.1
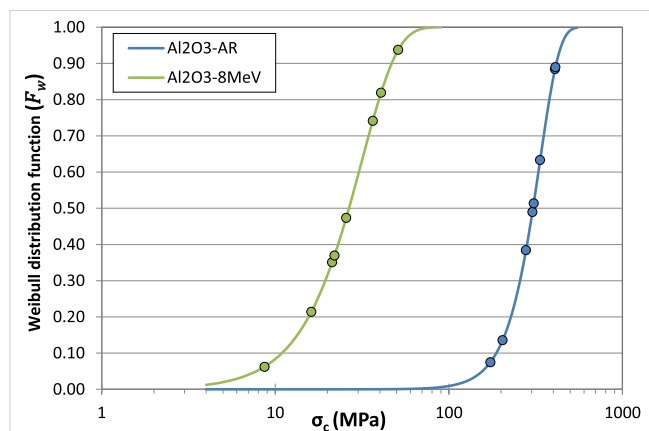
Fig. 4. The Weibull cumulative distribution function for the results of the compression tests. Blue and green referrers to the as-received, and ion-irradiated samples, respectively. (For interpretation of the references to colour in this figure legend, the reader is referred to the web version of this article.)

in Zaragoza, Spain, was used to prepare the TEM lamellae. To compare the irradiation-developed microstructures along the sample cross-section preparation, lamellae were FIB milled from the region of the beam incoming and outcoming surfaces, and in the middle of sample thickness (at around 100 μm), as shown in Fig. 3. Afterwards, FIB lamellae were thoroughly studied by transmission electron microscopy using a TEM JEOL 2100HT at 200 kV.
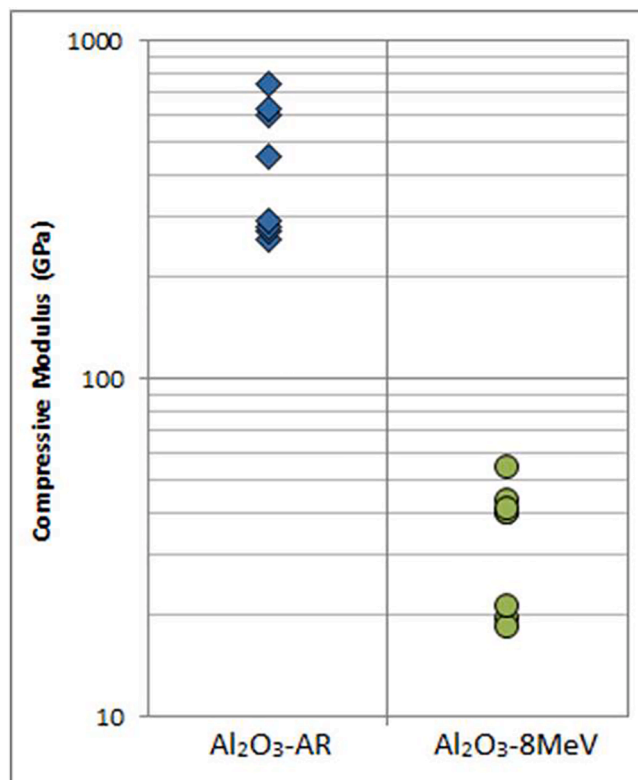
Fig. 5. The calculated compressive modulus of tested probes showing the scattering of values. Blue and green points refer to the as-received, and ion-irradiated samples, respectively. (For interpretation of the references to colour in this figure legend, the reader is referred to the web version of this article.)

Results

Compressive tests

In order to evaluate the detrimental effect in mechanical properties because of ions beam, the compressive properties of alumina were
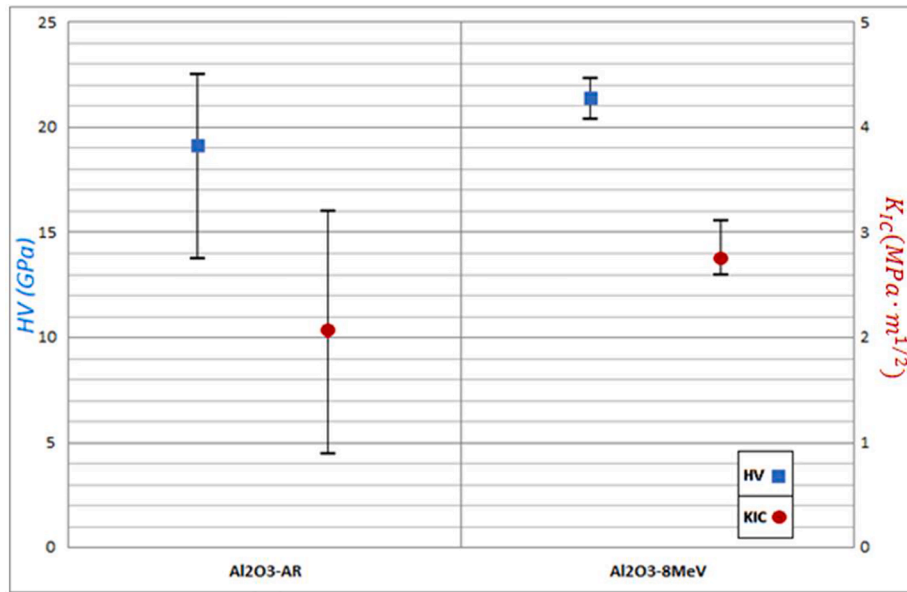
Fig. 6. Vickers hardness (blue squares) and fracture toughness (red circles) values were calculated from micro-indentation tests on the as-received alumina (left) and ion-irradiated samples (right). (For interpretation of the references to colour in this figure legend, the reader is referred to the web version of this article.)

evaluated in either the as-received and after irradiation state. To determine the compressive strength σ_C, compressive modulus E_C, and elastic energy from the experimentally obtained compression stress--strain curves, eight as-received and ion-irradiated probes were tested. Table 1 summarizes the mean mechanical values and the standard deviation, while Fig. 4 compares the cumulative function of the Weibull distributions for the AR and 8 MeV probes. The probability of failure evaluated by the cumulative Weibull distribution indicates that the larger the value of **m**, the smaller the resistance range, thus the smaller the number of defects appearing in the material. After irradiation of high-energy ions, the value of the Weibull modulus decreased with respect to the material in the as-received state, indicating the generation of defects in the material produced by the ions.

The elastic modulus obtained in each prismatic sample was compared in Fig. 5 according to the as-received or ion-irradiated group. The strength, modulus, and elastic energy of the samples irradiated with high-energy ions up to a fluence of 1.36×10^{16} ions/cm^2 show substantial changes in their compression behaviour. This observation makes this material quite unreliable for future breeding blanket applications.

Results of micro-indentation tests

The hardness (**H**) and fracture toughness (**K$_{IC}$**) of a ceramic material depend on a property known as brittleness, which is the inability of the material to deform plastically before cracking. The behaviour of alumina to Vickers-type micro-indentation tests is here studied comparatively between the as-received and the irradiated conditions.

After measuring the diagonal Vickers imprint and the cracks lengths
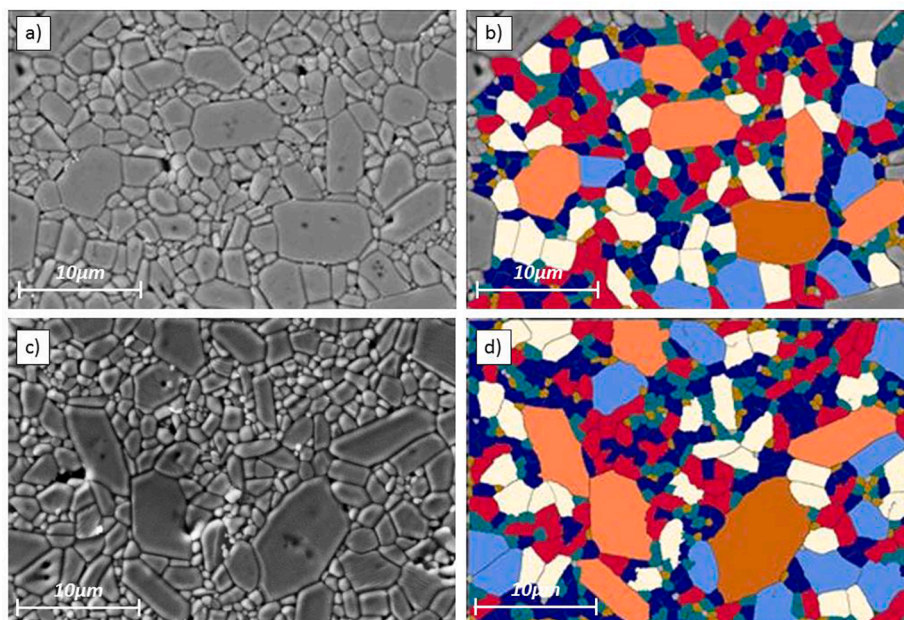
Fig. 7. SEM secondary electron images of polished and etched Al$_2$O$_3$ as-received (a) and high-energy ion-irradiated sample (c), and the resultant image after implementing the LAS grain analysis software for the as-received (b) and ion-irradiated sample (d).
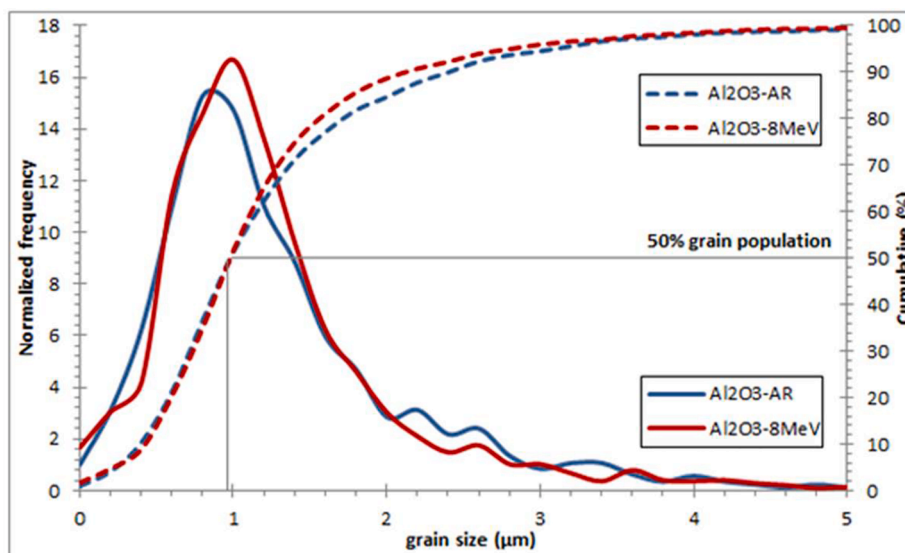
Fig. 8. Grain size distribution for the as-received (Al$_2$O$_3$-AR in blue) and ion-irradiated (Al$_2$O$_3$ – 8 MeV in red) samples. At 50% of the accumulated population, the grain size is 0.95 ± 0.1 μm. (For interpretation of the references to colour in this figure legend, the reader is referred to the web version of this article.)
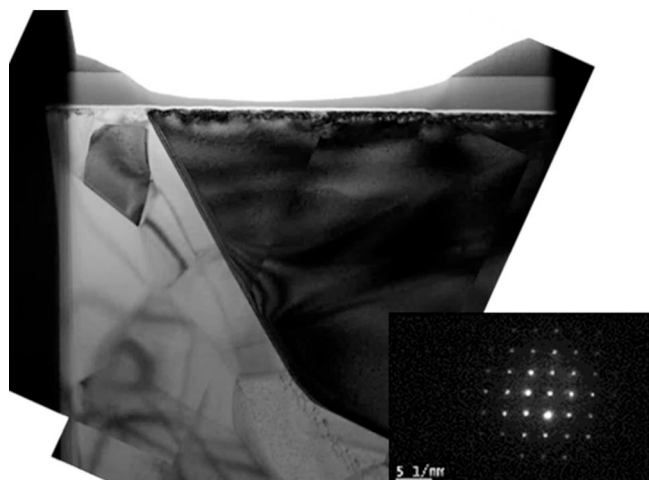
Fig. 9. TEM micrograph of the high-energy ion-irradiated sample FIB milled at the centre of sample thickness.

generated by the micro-indentation, the Vickers hardness **H** and the fracture toughness, **K$_{IC}$** were determined [14]. Fig. 6 shows the maximum, minimum, and average values obtained for the as-received (AR) and ion-irradiated (8 MeV) conditions probes. When comparing the results, the trend indicates that a fluence of 1.63×10^{16} ions/cm^2 produces a slight increase on both mentioned properties. Furthermore, a smaller distribution of the experimental calculated values is obtained, which is in agreement with the fact that no relationship with the position of the imprints in the width of the specimen has been observed. According to the SRIM simulation Fig. 1, the ion beam would penetrate the specimen, leaving homogeneous damage along with the 250 μm thickness of the specimen.

SEM microstructural study.

The mirror-like polishing cross-sectional surface of the samples was analyzed with the FESEM microscope after revealing the grain boundaries to verify the possible interaction of high-energy protons with the alumina microstructure. Fig. 7 **a** and **c** show the secondary electron micrographs of the as-received and ion-irradiated samples, respectively.

Both images show a similar monophasic microstructure with a large grain size distribution. Fig. 7 **b** and **d** depict the same microstructure after implementing the digitization program. The applied *LAS* analytical software assigns different colour according to the grain size, allowing an accurate average grain size measurement when the ASTM E112 standard method is followed. The resultant size of approximately 1000 grains is represented in Fig. 8 as a function of normalized frequency and accumulated fraction for both as-received and ion-irradiated samples. After calculating the grain size at 50% of the accumulated population, no evidence of change in the grain size was detected due to high energy ion irradiation, with 0.95 ± 0.1 μm being the value determined for the alumina material.

TEM microstructural study

Amorphization due to ion-irradiation in ceramics is one of the most common effects. Therefore, the orientation of grains existing in the FIB-milled lamellae were analyzed, trying to find sign of crystallographic distortions. However, no indication of amorphization or texture was observed. Fig. 9 shows an overview of the lamella extracted at the middle of the ion path. Several grains of different sizes were found randomly oriented. As an example, to take the image on Fig. 9 the sample was tilted to place the largest dark grain under zone-axis condition. The electron diffraction pattern, also shown in Fig. 9, concludes that no amorphization was produced in the alumina grains by the impinging of high-energy protons.

Nevertheless, a higher density of small cavities has been detected in the lamella extracted from the region at the projected range of the high-energy ions. Cavities nucleated within the matrix were detected throughout sample thickness regardless the impinging ion depth. As an example of the mentioned observation, a set of images is shown in Fig. 10 **b** to **10 d**. For comparison, the absence of cavities in the lamella extracted from the as-received material is shown in Fig. 10a. Furthermore, the density of cavities seems to increase almost proportionally with the amount of hydrogen implanted, which starts being significant from 150 μm in-depth as the simulated profile in Fig. 1 predicts. In this region, a random distribution of cavities within the matrix is found, where a likely alignment appears to be followed, as highlighted with yellow arrows in Fig. 10**d**.

Grain boundaries seem to be a relevant microstructural feature. Cavities were observed attached at grain boundaries, acting as defect sinks Fig. 11. In addition, randomly nucleated large cavities inside the
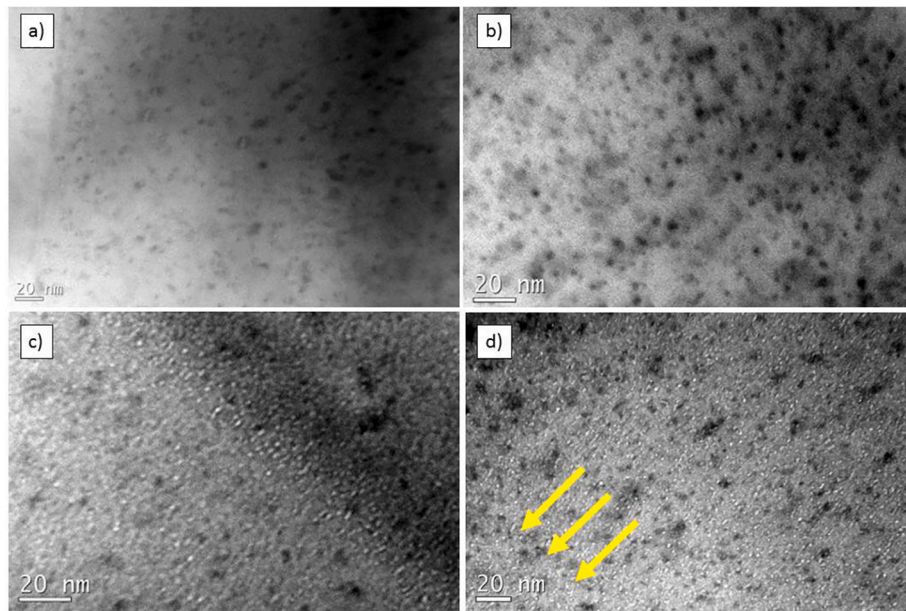
Fig. 10. TEM images showing the evolution of ion-induced cavity density in alumina material as a function of lamella position: at the ion incident surface, in the middle of sample thickness, and end of ion path (b, c, d), respectively. No cavities are depicted in the as-received alumina (a). Yellow arrows in image d point cavities fashion following a particular direction. (For interpretation of the references to colour in this figure legend, the reader is referred to the web version of this article.)
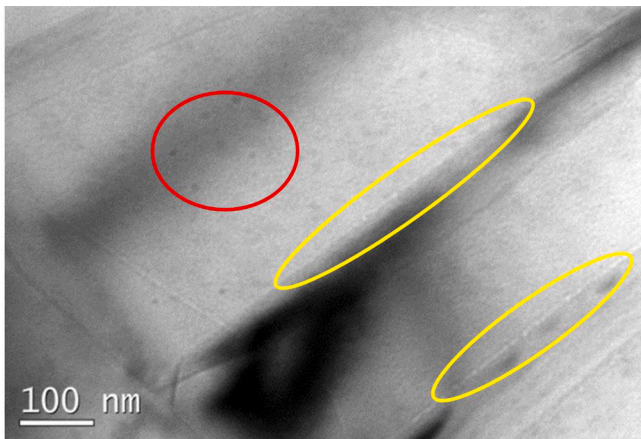
Fig. 11. TEM image showing the grain boundaries in the microstructure of the lamella milled at the projected range of the irradiated alumina sample. Yellow circles highlight grain boundaries acting as cavities or defects sink. The red circle shows relatively large cavities nucleating randomly in the grains. (For interpretation of the references to colour in this figure legend, the reader is referred to the web version of this article.)

Fig. 12. TEM image showing the dislocation loops observed in the alumina material exposed to the high-energy ion beam.

alumina grains were also detected in smaller quantities, as shown highlighted in the red circle in Fig. 11.

Finally, large dislocation loops were observed aligned within the matrix Fig. 12, likely attached to a non-visible microstructural feature due to the diffraction condition. In addition, a high density of defects, presumably large interstitial clusters or small loops, are observed in the same micrograph.

Discussion

For fusion applications, changes in mechanical properties of structural materials and their relationship with the microstructure have already been studied using different irradiation sources (ion implantation, fission neutrons, or spallation) [4,5,6,15,16,17,18] and explained as due to the nucleation and growth of radiation-induced cavities. In this

paper, to understand the behaviour and origin of variations on the mechanical properties produced by proton irradiation of commercial alumina are also discussed on a microstructural basis.

Due to the reduced thickness needed to achieve the total ion transmission required on the alumina probes, the compressive results obtained from ion-irradiated are here compared with data also obtained experimentally for the as-received alumina with similar thickness. Data reported by the manufacturer and the consulted literature [19] on the volumetric material should not be applied since defects induced during samples preparation may cause strength reduction [20]. Therefore, in order to reduce the stresses produced during machining, the thinned and polished specimens were thermally annealed.

It was known beforehand that radiation modified the mechanical properties of ceramics [16,21]. However, the low variation of the micro-indentation results here obtained in comparison to the significant change in the compression properties evaluated after alumina probes exposition to high-energy ion-irradiation was not expected. Nevertheless, this behaviour can be explained taking into account that compressive strength and fracture toughness are independent of each

other. Compressive strength is mainly determined by a crack initiation process, leading by plastic behaviour and not by crack propagation [18].

Katano [16] and Sasajima [17], among others, have already mentioned the changes observed using TEM in the microstructural defects of alumina samples after exposition to high-energy ion-irradiation, which are in good agreement with the results obtained in this research at RT. Regarding mechanical properties degradation, it can be explained due to radiation-induced anisotropic grain swelling accompanied by generation of internal stresses and production of cracks and grain decohesion at grain boundaries. However, SEM observations, where a large cross-sectional area was covered searching defects, cracks are found in both as-received and irradiated samples, being difficult to determine whether the defects found are a product of irradiation or due to the material manufacturing process. In this study, if changes in the microstructure are not noticeable by SEM is likely due to the lower fluences used. Likely, the dose threshold for which large-scale defects are effective has not been reached. Nevertheless, after the SEM study it is indicated that this slip-cast alumina retains the monomodal distribution without changes in the average grain size after ion-irradiation, at least up to a fluence of 1.63×10^{16} ions/cm^2, the value calculated at 50% of the accumulated population being 0.95 ± 0.1 μm.

According to the revised literature [4,6,22], changes in the mechanical properties of compression and micro-indentation could be satisfactorily explained due to the limited hydrogen solubility in ceramics. Therefore, the increase in fracture toughness, accompanied by the reduction in the compressive strength, is likely related to the formation and growth of cavities at the grain boundaries. Under the experimental conditions achieved in our work, a high density of cavities and the existence of dislocation loops are defects evidenced by TEM observations in the lamellae milled at different depths from the proton radiation impinging surface. Actually, nucleation of rather alligned (both random and quasi-preferential) cavities within the alumina matrix is found in a greater extent in the FIB lamella extracted at the end of the ion beam path. Furthermore, a large number of cavities are observed at the grain boundaries, which seem to act as defect sinks. Other authors [16,17] also point out this grain boundary effect in ion-induced cavities, mainly emphasizing in the cavity size enhancement at irradiation temperatures above 600 °C. Therefore, it is not surprising to measure an average cavity diameter close to 10 nm in this alumina irradiated at room temperature. The existence of even small-sized cavities or defects at grain boundaries may lead to local changes in the inter-grain compaction (grains decohesion), to a less efficient transmission of the mechanical stress, and thus may imply significant variations in the mechanical properties of the material.

Conclusions

The effects produced by high-energy ion-irradiation on the mechanical properties and the microstructure of commercial alumina manufactured by slip casting have been evaluated. Mechanical compression and micro-indentation tests have been performed to determine the strength, elastic modulus, hardness, and fracture toughness of alumina probes in the as-received and ion-irradiated conditions. Characterization results were compared between the as-received and ion-irradiated samples and explained in terms of SEM and TEM observations of the microstructure.

A total fluence of 1.63×10^{16} ions/cm^2 of proton irradiation produces relevant changes in the compression behaviour of alumina. Besides, hardness and fracture toughness slightly improve after irradiation, therefore allow concluding the mechanical resistance of this material to moderate ion irradiation fluences. The SEM microstructural study reveals the absence of changes in the grain size and the induction of other features (cracks, defects, …) due to high-energy proton irradiation. However, TEM study reveals the presence of cavities and dislocation loops mainly concentrated near the grain boundaries, caused by the transmitted proton beam. Furthermore, the defect density increases as

the TEM lamella is milled from positions in the specimen thickness close to the ion beam projected range. Grain boundaries seem to act as sinks of radiation-induced defect, which may help to diminish the microstructural damage and, hence, the mechanical degradation. This special arrangement of defects confers higher radiation tolerance to this commercial alumina, at least up to proton fluences of 1.63×10^{16} ions/cm^2.

References

[1] D. Rapisarda, I. Fernandez, I. Palermo, F.R. Urgorri, L. Maqueda, D. Alonso, T. Melichar, O. Frýbort, L. Vála, M. Gonzalez, P. Norajitra, H. Neuberger, A. Ibarra, Status of the engineering activities carried out on the European DCLL, Fusion Eng. Des. 124 (2017) 876–881, https://doi.org/10.1016/j.fusengdes.2017.02.022.

[2] S. Smolentsev, N.B. Morley, M.A. Abdou, S. Malang, Dual-coolant lead–lithium (DCLL) blanket status and R&D needs, Fusion Eng. Des. 100 (2015) 44–54, https://doi.org/10.1016/j.fusengdes.2014.12.031.

[3] F.R. Urgorri, S. Smolentsev, I. Fernández-Berceruelo, D. Rapisarda, I. Palermo, A. Ibarra, Magnetohydrodynamic and thermal analysis of PbLi flows in poloidal channels with flow channel insert for the EU-DCLL blanket, Nucl. Fusion 58 (10) (2018) 106001, https://doi.org/10.1088/1741-4326/aad299.

[4] S.J. Zinkle, Effect of H and He irradiation on cavity formation and blistering in ceramics, Nucl. Instrum. Methods Phys. Res., Sect. B 286 (Sep. 2012) 4–19, https://doi.org/10.1016/j.nimb.2012.03.030.

[5] S.J. Zinkle, G.S. Was, Materials challenges in nuclear energy, Acta Mater. 61 (3) (Feb. 2013) 735–758, https://doi.org/10.1016/j.actamat.2012.11.004.

[6] S. Furuno, N. Sasajima, K. Hojou, K. Izui, H. Otsu, T. Matsui, Radiation effects on Al2O3 irradiated with H2+ ions, J. Nucl. Mater. 258–263 (1998) 1817–1821, https://doi.org/10.1016/S0022-3115(98)00408-5.

[7] I. Fernández-Berceruelo, I. Palermo, F.R. Urgorri, Á. García, D. Rapisarda, L. Moya, F. Rueda, D. Alonso, Á. Ibarra, Alternatives for upgrading the EU DCLL breeding blanket from MMS to SMS, Fusion Eng. Des. 167 (2021) 112380, https://doi.org/10.1016/j.fusengdes.2021.112380.

[8] D. Rapisarda, I. Fernández-Berceruelo, A. García, J.M. García, B. Garcinuño, M. González, C. Moreno, I. Palermo, F.R. Urgorri, A. Ibarra, The European Dual Coolant Lithium Lead breeding blanket for DEMO: status and perspectives, Nucl. Fusion 61 (11) (2021) 115001, https://doi.org/10.1088/1741-4326/ac26a1.

[9] A. Redondo-Cubero, M.J.G. Borge, N. Gordillo, P.C. Gutiérrez, J. Olivares, R. Pérez Casero, M.D. Ynsa, Current status and future developments of the ion beam facility at the centre of micro-analysis of materials in Madrid, Eur. Phys. J. Plus 136 (2) (2021), https://doi.org/10.1140/epjp/s13360-021-01085-9.

[10] R.E. Stoller, M.B. Toloczko, G.S. Was, A.G. Certain, S. Dwaraknath, F.A. Garner, On the use of SRIM for computing radiation damage exposure, Nucl. Instrum. Methods Phys. Res., Sect. B 310 (2013) 75–80, https://doi.org/10.1016/j.nimb.2013.05.008.

[11] F. Mota, C.J. Ortiz, R. Vila, N. Casal, A. García, A. Ibarra, Calculation of damage function of Al2O3 in irradiation facilities for fusion reactor applications, J. Nucl. Mater. 442 (1–3) (2013) S699–S704, https://doi.org/10.1016/j.jnucmat.2012.11.002.

[12] W.J. Weber, Y. Zhang, Predicting damage production in monoatomic and multi-elemental targets using stopping and range of ions in matter code: Challenges and recommendations, Curr. Opin. Solid State Mater. Sci. 23 (4) (2019) 100757, https://doi.org/10.1016/j.cossms.2019.06.001.

[13] S. Chen, D. Bernard, On the calculation of atomic displacements using damage energy, Results Phys. 16 (2020) 102835, https://doi.org/10.1016/j.rinp.2019.102835.

[14] A.G. Evans, E.A. Charles, Fracture toughness determinations by indentation, J. Am. Ceram. Soc. 59 (7-8) (1976) 371–372, https://doi.org/10.1111/j.1151-2916.1976.tb10991.x.

[15] M. Roldán, P. Galán, F. José Sánchez, I. García-Cortés, D. Jiménez-Rey, P. Fernández, Ion beam experiments to emulate nuclear fusion environment on structural materials at CMAM, in: I. Ahmad, T. Zhao (Eds.), Ion Beam Techniques and Applications, IntechOpen, 2020, https://doi.org/10.5772/intechopen.87054.

[16] Y. Katano, T. Aruga, S. Yamamoto, T. Nakazawa, D. Yamaki, K. Noda, Cross-sectional observation of damage structures in Al2O3 irradiated with multiple beams of H, He, and O ions and after annealing at 1273 K, Nucl. Instrum. Methods Phys. Res., Sect. B 140 (1–2) (Apr. 1998) 152–158, https://doi.org/10.1016/S0168-583X(97)00925-7.

[17] N. Sasajima, T. Matsui, S. Furuno, K. Hojou, H. Otsu, Damage accumulation in Al2O3 during H2+ or He+ ion irradiation, Nucl. Instrum. Methods Phys. Res., Sect. B 148 (1–4) (1999) 745–751, https://doi.org/10.1016/S0168-583X(98)00810-6.

[18] W. Dienst, Mechanical properties of neutron-irradiated ceramic materials, J. Nucl. Mater. 211 (3) (1994) 186–193, https://doi.org/10.1016/0022-3115(94)90346-8.

[19] P. Auerkari, Mechanical and Physical Properties of Engineering Alumina Ceramics, VTT Technical Research Center of Finland, Espoo, 1996.

[20] G. Sines, M. Adams, Compression Testing of Ceramics, in: R.C. Bradt, D.P. H. Hasselman, F.F. Lange (Eds.), Flaws and Testing, Springer US, Boston, MA, 1978, pp. 403–434, 10.1007/978-1-4615-7017-2_23.

[21] F.W. Clinard, W. Dienst, E.H. Farnum, Issues related to mechanical properties of neutron-irradiated ceramics, J. Nucl. Mater. 212–215 (1994) 1075–1080, https://doi.org/10.1016/0022-3115(94)90998-9.

[22] W. Dienst, H. Zimmermann, Fracture toughness and strength change of neutron-irradiated ceramic materials, J. Nucl. Mater. 212–215 (1994) 1091–1095, https://doi.org/10.1016/0022-3115(94)91001-4.